STUDY ON VIBRATION CHARACTERISTICS OF DAMPING BLADE WITH SNUBBER AND SHROUD BASED ON FRACTAL THEORY

by

Wei ZHAO, Liang-Liang LI, and Di ZHANG*

Ministry of Education Key Laboratory of Thermo-Fluid Science and Engineering, School of Energy and Power Engineering, Xi'an Jiaotong University, Xi'an, China

Original scientific paper
DOI: 10.2298/TSCI160201205Z

Snubber and shroud have been widely adopted in steam turbine last stage blades to decrease the vibration stress. The contact surfaces between snubber and shroud own obviously fractal geometry characteristics. Based on fractal geometry theory and finite element non-linear vibration theory, the fractal friction model that describes friction damping contact could be accurately established. In this paper, the contact fractal elements are set up and the non-linear vibration response characteristics of a long steam turbine last stage blade with snubber and shroud are calculated. The results show that, with the increase of shroud normal force, the resonant amplitude of the blade experiences a decreasing period followed by an increasing period while the modal damping ratio increases first and then decreases when there is only shroud contact. The regulations are similar when there are both shroud and snubber contacts. The resonant frequency increases until the normal contact forces increase to some degree.

Key words: *steam turbine blade, fractal theory, friction damping, vibration characteristics*

Introduction

With the development trend toward high parameter and large capacity, the exciting force loaded on steam turbine blades increases significantly. The blade vibrates intensively and is prone to high cycle fatigue failure [1]. An effective way is to adopt an integral snubber and shroud damping structure in the design of the blade to improve the rigidity and damping of the system. The friction contact surfaces of blades have friction damping characteristics. The complex contact state brings great difficulties to the vibration analysis of the blade.

Scholars have put forward a variety of contact friction damping model to describe the friction damping characteristics in contact interfaces, but no accurate results were obtained. Friction damping models based on the Hertz theory were generally adopted. Damping structures of the blade, such as lacing wire, integral shroud, and dampers, have been widely researched for the vibration characteristic. Menq *et al.* [2] proposed a friction contact model that could investigate the stuck-sliding-separated state between the contact surfaces when the normal force changes. Yang *et al.* [3] further proposed a more complex friction analysis model that judge the stuck-sliding-separated state, and a theoretical formula transformed between the various contact states was deduced under the condition of simple harmonic motion. Ciger-

* Corresponding author; e-mail: zhang_di@mail.xjtu.edu.cn

oglu *et al.* [4] proposed a 1-D dynamic microslip friction model, which considered the friction damper inertia, and the different viscous-sliding state transition process with three different normal force distributions was analyzed.

Fractal geometry theory has been widely used to analyze the engineering structure surfaces and contact stiffness with scale invariance and self-affinity [5-9]. Though blade friction damping contact surfaces seem to be complex and disordered, actually they show the same features of fractal behavior and complex non-linearity. Friction model based on the fractal geometrical theory gradually attracts the attention of scholars. Jiang *et al.* [10] proposed a general contact stiffness model to study the contact state between rough surfaces of machined plane joints under different normal load by fractal theory and experimentally verified the method. Liu *et al.* [11] used the fractal theory to investigate the non-linear vibration behavior of a shrouded blade with friction dynamic contact interface.

Based on the fractal geometry theory and finite element non-linear vibration theory, a friction damping vibration analysis model of a last stage long steam turbine blade with snubber and shroud is built in this paper. By programing APDL and combining software ANSYS, we calculate the vibration response characteristics of the blade through iterative computations under different normal forces in snubber and shroud contact interfaces.

Fractal contact model and finite element method

Fractal contact model and contact stiffness

Local contact surfaces of the blade display self-similarity. Whether which scale observed from, there are similar fine structures in a smaller scale in the surface, which can be characterized by fractal geometry. Fractal contact surface cannot describe the internal structure by characteristic scale, and it generally depends on the concept of the fractal similar dimension.

Assuming that an object or geometry has the characteristics of fractal geometry, it can be divided into N parts and each part has the self-similarity. Thus, the fractal similar dimension D can be written:

$$D = \frac{\ln N}{\ln \frac{1}{r}} \tag{1}$$

where r is the scale length and N is the scale number.

Contact surface roughness can be deterministically simulated by W-M function, which can be expressed [6, 7, 12-14]:

$$z(x) = L\left(\frac{G'}{L}\right)^{D-1} \sqrt{\ln \beta} \sum_{n=0}^{n_{\max}} \beta^{(D-2)n} \left[\cos \phi_{1,n} - \cos\left(\frac{2\pi\beta^n x}{L} - \phi_{1,n}\right)\right] \tag{2}$$

where z is the random surface profile height, x – the displacement co-ordinate distance, G' – the fractal roughness characteristic scale reflecting the size of z, D – the fractal dimension ($1 < D < 2$), quantitatively measuring the irregular and complexity of surface profile on all scales, $\phi_{1,n}$ – a random phase, β – a constant greater than 1 which determines the spectral density and the scale of the self-similarity (for a random surface that obeys the normal distribution, $\beta = 1.5$ [10]), β^n – the spatial frequency controlling the spectrum of rough surface, and L – the sample length.

The normal contact stiffness of a microcontact can be written [10]:

$$k_n = \frac{\mathrm{d}F}{\mathrm{d}\delta} = \frac{4E^*}{3\sqrt{\pi}} \frac{3-D}{2-D} \sqrt{a} \tag{3}$$

where E^* and a denote the equivalent elastic modulus of system and the real microcontact area, respectively, and F is the normal contact force.

The tangential stiffness of a microcontact is expressed [10]:

$$k_\tau = \frac{4Gr_s}{2-v} \tag{4}$$

where G, r_s, and v denote the shear modulus of elasticity, radius of real contact area and Poisson ratio, respectively.

Thus, the whole normal stiffness K_n and the whole tangential stiffness K_τ are given by [10]:

$$K_n = \int_{a_c'}^{a_l'} k_n n(a') \mathrm{d}(a') = \frac{4D(3-D)E^*}{3\sqrt{2\pi}(2-D)(D-1)} [a_l'^{(D/2)} a_l'^{(1-D/2)} - a_l'^{(1/2)}] \tag{5}$$

$$K_\tau = \int_{a_c'}^{a_l'} k_\tau n(a') \mathrm{d}(a') = \frac{4DE^*(1-v)}{\sqrt{2\pi}(2-v)(D-1)} [a_l'^{(D/2)} a_l'^{(1-D/2)} - a_l'^{(1/2)}] \tag{6}$$

Finite element non-linear vibration method

The partial differential equation of system motion can be expressed by:

$$[\mathrm{M}] \frac{\partial^2 \delta}{\partial t^2} + [\mathrm{M_G}] \frac{\partial \delta}{\partial t} + \zeta^T [\mathrm{H}] \zeta \delta = \vec{\mathrm{F}} + \vec{\mathrm{Q}}_\mathrm{C} + \vec{\mathrm{Q}}_\mathrm{p} \tag{7}$$

where [M] is the element mass matrix, $[\mathrm{M}_G]$ – the element Corolis force matrix, ζ – the partial differential factor, [H] – the constitutive matrix, $\vec{\mathrm{F}}$ – the node force vector given by the adjacent element and the boundary condition of the blade, $\vec{\mathrm{Q}}_C$ – the centrifugal force vector of element, and $\vec{\mathrm{Q}}_p$ – the aerodynamic force vector of element.

The partial differential factor ζ can be expressed:

$$\zeta = \begin{bmatrix} \frac{\partial}{\partial x} & & & \frac{\partial}{\partial y} & & \frac{\partial}{\partial z} \\ & \frac{\partial}{\partial y} & & \frac{\partial}{\partial z} & \frac{\partial}{\partial x} & \\ & & \frac{\partial}{\partial z} & & \frac{\partial}{\partial y} & \frac{\partial}{\partial x} \end{bmatrix}^T \tag{8}$$

According to finite element method to assemble, eq. (7) could be written:

$$[\mathrm{M}] \frac{\partial^2 \delta}{\partial t^2} + [\mathrm{M}]_\mathrm{G} \frac{\partial \delta}{\partial t} + \zeta^T [\mathrm{H}] \zeta \delta = \sum \vec{\mathrm{F}} + \sum \vec{\mathrm{Q}}_\mathrm{C} + \sum \vec{\mathrm{Q}}_\mathrm{p} \tag{9}$$

When the structure system motion equation is large and the dynamic response calculation costs a long time, the multimode solution method is employed generally. The n^{th} normalized mode shape can be written as the following form:

$$\Psi = [\psi_1 \quad \psi_2 \quad \cdots \quad \psi_n] \tag{10}$$

The displacements can be obtained:

$$\delta = \Psi[q] = [\psi_1 \quad \psi_2 \quad \cdots \quad \psi_n] \times [q_1 \quad q_2 \quad \cdots \quad q_n]^T \tag{11}$$

where $[q]$ is a single column matrix of co-ordinate values.

Multiplying eq. (9) by Ψ^T, the equation of system motion can be formulated:

$$[\mathrm{I}]\frac{\partial^2 q}{\partial t^2} + \Psi^T[\mathrm{M}]_\mathrm{G}\Psi\frac{\partial q}{\partial t} + \Psi^T\zeta^T[\mathrm{H}]\zeta\Psi q = R \tag{12}$$

where $R = \Psi^T(\Sigma\vec{\mathrm{F}} + \Sigma\vec{\mathrm{Q}}_\mathrm{C} + \Sigma\vec{\mathrm{Q}}_\mathrm{p}) = [r_1 \quad r_2 \quad \cdots \quad r_n]^T$.

Equation (12) indicates n mutual independent second-order partial differential equations. When the damping ratio is very small, q_i can be calculated by:

$$q_i = \frac{1}{\omega_i}\int_0^t r_i \sin\omega_i(t-\tau)\mathrm{d}\tau + a_i \sin\omega_i t + b_i \cos\omega_i t \tag{13}$$

where a_i and b_i are constants determined by the initial conditions, ω_i – the natural frequency and τ – a time increment, which is less than t.

Substituting eq. (13) into eq. (12), the response displacement can be represented:

$$\delta = \sum_{i=1}^{n} \psi_i q_i \tag{14}$$

Response analysis of a friction damping blade

The finite element model (FEM) of the last stage long steam turbine blade with snubber and shroud is established, as illustrated in fig. 1. The friction damping structures of the blade include the shroud located at the top and the snubber located at 50% blade height. The friction damping effects between adjacent snubber and shroud surfaces, for one thing, increase the stiffness and avoid the resonance, for another, dissipate the vibration energy and increase the structure damping.

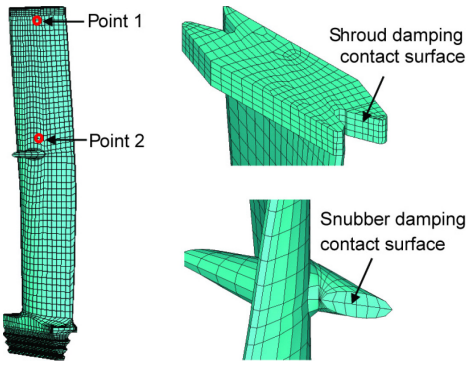

Figure 1. The FEM model of a long steam turbine blade with snubber and shroud

The 3-D non-linear contact analysis of the blade is carried out in 18 operating conditions ranging from 2100 rpm to 3000 rpm. Through further analysis, the normal forces in snubber and shroud friction interfaces under different speeds are obtained, which provides the basis for the analysis of vibration response characteristics. Figure 2 shows the changing curves of the normal

force between the adjacent snubber and shroud contact surfaces along with the change of rotational speed. It can be seen that, the normal force between the shroud surfaces increases with the speed. Besides, after snubber surfaces closes at 2413 rpm, the normal force between the snubber contacts increases with the speed.

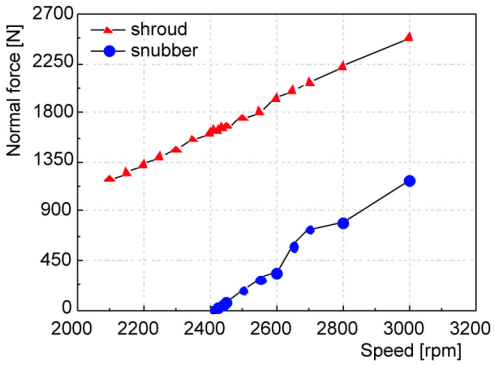

Figure 2. Changing patterns of normal force between snubber and shroud surfaces

Spring damping elements are built in the snubber and shroud interfaces to simulate the friction damping effect. Analysis of vibration characteristics of the damping blade based on fractal theory is carried on under a variety of normal force conditions corresponding to different rotational speeds. The response curves of the vibration amplitude of point 1 and point 2 of the blade are obtained. Point 1 is at the top and point 2 is above the snubber center section.

By introducing dimensionless vibration displacement, γ, in the result analysis, the vibration amplitude of the response curve is converted into the corresponding dimensionless quantity. Dimensionless vibration displacement γ can be written:

$$\gamma = \frac{A}{A_\gamma} \tag{15}$$

where A_γ is the resonant response amplitude of point 1 of free-standing blade, and A is the calculated resonant response amplitude.

Figures 3 and 4 show the numerical results of point 1 and point 2 under various conditions. While the blade contacts, the resonant amplitude of point 1 of friction damping blade decreases maximally to 1.37% of that of free-standing blade. The resonant amplitude of point 2 of friction damping blade decreases maximally to 7.64% of that of free-standing blade.

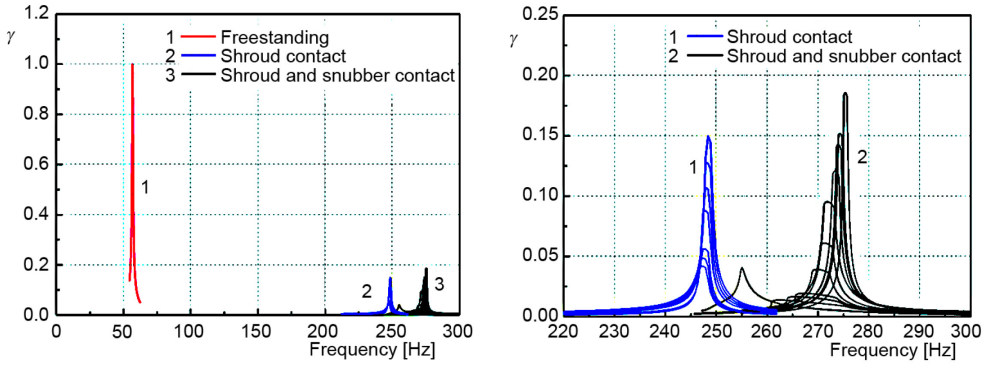

Figure 3. Calculation results of point 1; (a) the test response curves, (b) partial enlargement

To investigate the effects of friction damping between snubber and shroud surfaces on vibration characteristics of the blade, the frequency response curves of vibration amplitude are obtained under six different contact conditions from condition a-f, as shown in tab. 1.

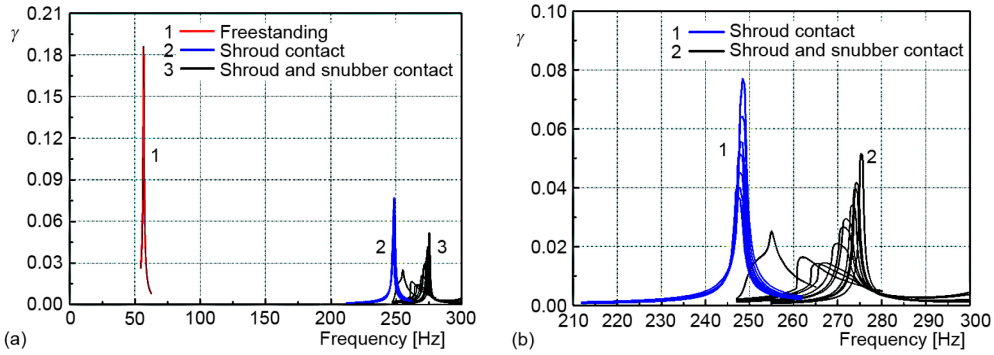

Figure 4. Calculation results of point 2; (a) the test response curves, (b) partial enlargement

Table 1. Test conditions

Conditions	Speed, [rpm]	Shroud normal force, [N]	Snubber normal force, [N]
a	0	0	0
b	2200	1311.4	0
c	2300	1454.3	0
d	2413	1628.6	12.3
e	2600	1921.4	340.7
f	3000	2475.7	1183.7

Figures 5 and 6 show the resultant curves of resonant amplitude and modal damping ratio along with the change of test condition. From conditions a-c, the resonant amplitude decreases first and then increases while the modal damping ratio increases first and then decreased. In condition a, the blade is free-standing, only relying on material damping to dissipate vibration energy, which leads to a greater resonant amplitude and a lower resonant damping. In condition b, vibration energy of the blade is dissipated mainly by friction movement in shroud contact interfaces, which decreases the resonant amplitude and increases the modal damping ratio. In condition c, although the increasing normal force in shroud contact interfaces gives rise to a higher friction, the relative movement displacement amplitude is also greatly reduced, which leads to the increase in resonant amplitude and the decrease in modal damping ratio.

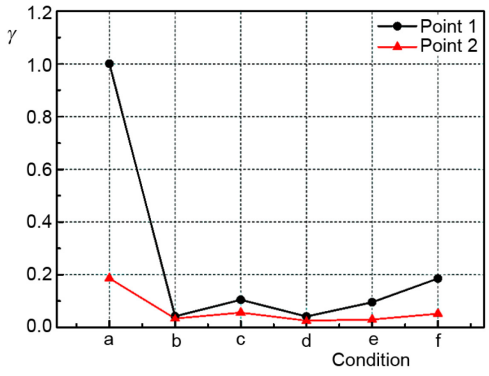

Figure 5. Changing curves of resonant amplitude for point 1 and point 2

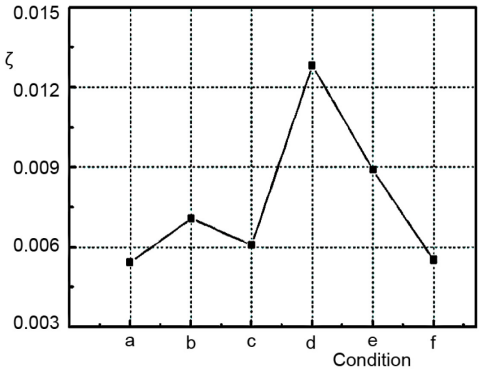

Figure 6. Changing curve of modal damping ratio

It can also be seen that, from condition c-f, there are both shroud and snubber contacts and the resonant amplitude decreases first and then increases gradually, while the modal damping ratio increases first and then decreased gradually. The normal force between shroud surfaces is high and the vibration energy is dissipated mainly in snubber interface. The normal force in snubber interfaces increases as the test condition changes, which brings that the changing patterns of the resonant amplitude and the modal damping ratio are similar to that at the previous stage.

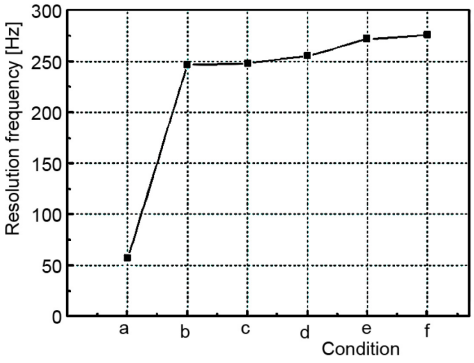

Figure 7. Changing curve of resonant frequency

Figure 7 shows the resultant curve of resonant frequency along with the change of the test conditions. From conditions a-f, the resonant frequency of the blade increases continuously. The resonant frequency changes highly at low normal force, and it changes little at high normal force. After condition e, blade interfaces of shroud and snubber are in a viscous state, which means the blade is self-locked and leads to the little variation in resonant frequency.

Conclusions

Based on the fractal geometry theory and finite element non-linear vibration theory, a fractal contact model of the blade is set up. By using the analysis method of vibration damping response steam turbine blade with snubber and shroud, the analysis of friction damping vibration response characteristics of a large power long steam turbine last stage blade with snubber and shroud is carried out. Snubber surfaces close at 2413 rpm and normal forces between the snubber and shroud surfaces increase with the speed. The resonant amplitude of point 1 and point 2 of friction damping blade are maximally reduced to 1.37% and 7.64% of that of free-standing blade, respectively. With the increase of shroud normal force, the resonant amplitude of the blade experiences a decreasing period followed by an increasing period while the modal damping ratio increases first and then decreases when there is only shroud contact. The regulations are similar when there are both shroud and snubber contacts. The resonant frequency increases with normal forces. When the normal contact forces increase to some degree, the resonant frequency changes little.

Nomenclature

a – real micro-contact area, [m^2]
D – fractal similar dimension, [–]
E^* – equivalent elastic modulus, [Nm^{-1}]
F – normal contact force, [N]
G' – roughness characteristic scale, [–]
G – shear modulus of elasticity, [Nm^{-1}]
K_n – whole normal stiffness, [Nm^{-1}]
K_τ – whole tangential stiffness, [Nm^{-1}]
k_n – normal stiffness, [Nm^{-1}]
k_τ – tangential stiffness, [Nm^{-1}]
L – sample length, [m]
q – matrix of co-ordinate values, [–]
r_s – radius of real contact area, [m]
z – surface profile height, [m]

Greek symbols

γ – dimensionless vibration displacement
δ – displacement, [m]
ζ – partial differential factor, [–]
ν – Poisson ratio, [–]
τ – time increment, [s]
Ψ – nth normalized mode shape, [–]
ω_i – natural frequency, [–]

References

[1] Zhao, Z. H., *et al.*, A Review of Research on Damper of Turbine Blade, *Turbine Technology*, *50* (2008), 1, pp. 1-5
[2] Menq, C. H., *et al.*, The Influence of a Variable Normal Load on the Forced Vibration of a Frictionally Damped Structure, *Journal of Engineering for Gas Turbines and Power*, *108* (1986), 2, pp. 300-305
[3] Yang, B. D., *et al.*, Stick-Slip-Separation Analysis and Non-Linear Stiffness and Damping Characterization of Friction Contacts Having Variable Normal Load, *Journal of Sound and Vibration*, *210* (1998), 4, pp. 461-481
[4] Cigeroglu, E., *et al.*, One-Dimensional Dynamic Microslip Friction Model, *Journal of Sound and Vibration*, *292* (2006), 3-5, pp. 881-898
[5] Majumdar, A., *et al.*, Fractal Characterization and Simulation of Rough Surfaces, *Wear*, *136* (1990), 2, pp. 313-327
[6] Majumdar, A., *et al.*, Fractal Model of Elastic-Plastic Contact Between Rough Surfaces, *Journal of Tribology*, *113* (1991), 1, pp. 1-11
[7] Yan, W., *et al.*, Contact Analysis of Elastic-Plastic Fractal Surfaces, *Journal of Applied Physics*, *84* (1998), 7, pp. 3617-3624
[8] Komvopoulos, K., Ye, N., Three-Dimensional Contact Analysis of Elastic-Plastic Layered Media with Fractal Surface Topographies, *Journal of Tribology*, *123* (2001), 3, pp. 632-640
[9] Goerke, D., *et al.*, Normal Contact of Fractal Surfaces Experimental and Numerical Investigations, *Wear*, *264* (2008), 7-8, pp. 589-598
[10] Jiang, S., Y., *et al.*, A Contact Stiffness Model of Machined Plane Joint Based on Fractal Theory, *Journal of Tribology*, *132* (2010), 1, pp. 1-7
[11] Liu, Y., L., *et al.*, A Friction Contact Stiffness Model of Fractal Geometry in Forced Response Analysis of a Shrouded Blade, *Non-Linear Dynamics*, *70* (2012), 3, pp. 2247-2257
[12] Borodich, F. M., *et al.*, Similarity and Fractality in the Modelling of Roughness by a Multilevel Profile with Hierarchical Structure, *International Journal of Solids Structures*, *36* (1999), 17, pp. 2585-2612
[13] Majumdar, A., *et al.*, Fractal Network Model for Contact Conductance, *Journal of Heat Transfer*, *113* (1991), 3, pp. 516-525
[14] Kogut, L., *et al.*, Electrical Contact Resistance Theory for Conductive Rough Surfaces, *Journal of Applied Physics*, *94* (2003), 5, pp. 3153-3162

Paper submitted: February 1, 2016
Paper revised: March 15, 2016
Paper accepted: March 26, 2016